Original article

β-Carboline copper complex as a potential mitochondrial-targeted anticancer chemotherapeutic agent: Favorable attenuation of human breast cancer MCF7 cells via apoptosis

Rais Ahmad Khan [a],*, Mohammad Rashid Khan [b], Mohammad Usman [c], Fatima Sayeed [d], Huda A. Alghamdi [e], Sulaiman Alrumman [e], Walaa Alharbi [f], Nida N. Farshori [g], Mai M. Al-Oqail [g], Mohd. Rafiq Siddiqui [a], Maymonah Abu Khanjer [a], Ali Alsalme [a]

[a] Department of Chemistry, College of Science, King Saud University, P.O. Box 2455, Riyadh 11451, Saudi Arabia
[b] Department of Pharmacology and Toxicology, College of Pharmacy, King Saud University, P.O. Box 2457, Riyadh 11451, Saudi Arabia
[c] Department of Chemistry, Indian Institute of Technology, Kanpur, India
[d] King Saud bin Abdul Aziz University for Health Sciences, Basic Science Department, College of Science and Health Profession, Al-Ahsa, Saudi Arabia
[e] Department of Biology, College of Sciences, King Khalid University, Abha, Saudi Arabia
[f] Department of Chemistry, Faculty of Science, King Khalid University, P.O. Box 9004 Abha, Saudi Arabia
[g] Department of Pharmacognosy, College of Pharmacy, King Saud University, P.O. Box 2457, Riyadh, 11451, Saudi Arabia

ARTICLE INFO

ABSTRACT

The development of preferentially selective cancer chemotherapeutics is a new trend in drug research. Thus, we designed and synthesized novel ternary complexes, $[Cu(tryp)(Hnor)_2(DMSO)]NO_3$ (**1**) and $[Zn(tryp)(Hnor)_2(DMSO)]NO_3$ (**2**) (tryp = DL-Tryptophane; Hnor = Norharmane, β-carboline; DMSO = Dimethyl sulfoxide), characterized with elemental analysis, FTIR, UV–vis, FL, NMR, ESI-MS, and molar conductivity. Furthermore, the TD-DFT studies with UV–vis and FTIR validated the proposed structures of **1** and **2**. Moreover, we evaluated the HOMO-LUMO energy gap and found that **1** has a smaller energy gap than **2**. Then, **1** and **2** were assessed for anticancer chemotherapeutic potential against cancer cell lines MCF7 (human breast cancer) and HepG2 (human liver hepatocellular carcinoma) as well as the non-tumorigenic HEK293 (human embryonic kidney) cells. The MTT assay illustrated the preferentially cytotoxic behavior of **1** when compared with that of **2** and cisplatin (standard drug) against MCF7 cells. Moreover, **1** was exposed to MCF7 cells, and the results indicated the arrest of the G2/M phases, which followed the apoptotic pathway predominantly. Generation of ROS, GSH depletion, and elevation in LPO validated the redox changes prompted by **1**. These studies establish the great potential of **1** as a candidate for anticancer therapeutics.

1. Introduction

Cancer is a foremost health hazard for humanity (Shaharyar et al., 2010). Despite immense advances in the field of basic and clinical research, which have resulted in higher cure rates for several malignancies, cancer remains one of the leading causes of death across the world. Although cancer mortality is second to heart disorders, the former is steadily rising, while the latter is leveling off. Since the discovery of cisplatin, the study of chemotherapeutics has majorly progressed, and a transition has been fostered by the inclusion of non-platinum metals, which display remarkable properties in terms of chemotherapeutic regimen. This evolution is much needed to overcome the adverse side effects of platinum-based drugs. It started as an alternative approach to investigate or design new chemotherapeutic agents, such as cisplatin, carboplatin, oxaliplatin, and satraplatin NAMI-A, with improved specificity, efficacy, and pharmacological properties (Hassouneh et al., 2007; Bruijnincx and Sadler, 2008; Xie and Kang, 2009; Ruiz-Azuara et al., 2010; Santini et al., 2014; Stefani et al., 2015; Ndagi et al., 2017).

Two of the most widely exploited transition metals in this field of study are Cu(II) and Zn(II) as both these metals possess a strong propensity towards protein and DNA. Cu, a transition element, is regarded as an essential trace element in the human body that plays vital roles in various metalloproteinases (Ndagi et al., 2017). It has been selected for the synthesis of antitumor drugs under the condition that it might yield lower systemic toxicity. A variety of N-, S-, or O-containing ligands have been designed and explored, which suitably bind with Cu(II) and Zn(II) and show potential antitumor activity. This can be attributed to the presence of N, O, and S donors, which leads to diverse biological potencies of these metal complexes. For example, the success of disulfiram in clinical trials is mainly attributed to its metabolite, a Cu-diethyldithiocarbamate complex, which binds NPL4 (nuclear protein localization protein 4) and induces its aggregation to eliminate cells (Chen et al., 2006; Festa and Thiele, 2011; Skrott et al., 2017). We recently found that a series of phenanthroline Cu(II) complexes exhibited potent anti-metastatic and anti-angiogenic activities against cancer cells (Shi et al., 2018). One recently studied complex includes coumarin-derived Schiff bases and their Cu(II) complexes, which exert toxicity in the breast cancer-zinc-derived MCF-7 mammalian cell line at concentrations that were comparable to the toxicity of the commercially used drug, mitoxantrone (Creaven et al., 2010). On the contrary, Zn(II) complexes also possess a wide range of chemotherapeutic potential, as evidenced by numerous earlier studies (Filipović et al., 2015; Huang et al., 2019; Lazou et al., 2019; Malarz et al., 2020; Mohanty et al., 2020). Both these metal complexes work via different mechanistic pathways to induce apoptosis or cell death. Thus, the anticancer activity of metal complexes is not only a measure of the variety of metal centers used but also depends on the type of ligand incorporated into the complex. Both these aspects go hand in hand while designing a potent chemotherapeutic agent. Induction of anticancer effects by any Cu(II) or Zn(II) complexes is a broad field of interest for inorganic medicinal chemists. Cu complexes are regarded as effective and frequently studied metallonucleases because of their exceptional biological oxidative/reductive potential. Thus, Cu complexes are widely known to follow a reactive oxygen species (ROS) mechanism of action for inducing apoptosis in cancerous cells. This was evidenced recently by a series of Cu complexes known as the "Casiopeina" series, which are considered remarkable as they initiate their anticancer effects through the ROS mechanism (Kachadourian et al., 2010). However, in cancer, ROS are present at high concentrations. In some types of cancers, owing to the high metabolic activities of cells (Redza-Dutordoir and Averill-Bates, 2016).

The design of the biocompatible organic moiety also plays a pivotal role in the efficacy of metal-based chemotherapeutics. Therefore, we have explored the planar biocompatible organic moiety, norharmane, which possesses the potential to pass through the blood–brain barrier. Norharmane (Hnor), 9H-pyrido [3,4-b] indole, is an unconventional ligand, belonging to an alkaloid family called β-carbolines (βCs). These molecules can act as a coordinating ligand, an H-bonding donor/acceptor, and may act at the level of π-π stacking (Khan et al., 2016). They have several biological efficacies, especially in eliminating cancer cells, which is why they are considered an exceptional ligand among medicinal chemists (Khan et al., 2016; Panice et al., 2019). Recently, our group explored β-carboline Co(II), Cu(II), Ni(II), and Zn(II) complexes with phenanthroline as the co-ligand for anticancer properties while also investigating the silver Hnor complexes' binding propensity with human serum albumin (HSA), the most abundant protein present in the body (Alsalme et al., 2018).

Thus, new therapeutic strategies need to be pursued that can selectively generate oxidative stress in cancer cells as a possible treatment for malignant cancers. This strategy, however, can only be realized when the designed metal-based drug is highly selective towards its target molecule. Another critical factor is the stability of complexes under aqueous and physiological conditions that ensure the potency of molecules interacting at the target sites and makes the molecule viable for further investigation and application. One possibility of doing so is by regulating the cellular response to different anticancer therapeutics by introducing modifications of glutathione (GSH) metabolism as well as agents that are able to modulate GSH concentrations in tumor cells. Nevertheless, these approaches have limited applicability due to harmful effects on normal cells. GSH is the most abundant antioxidant found in living organisms and has multiple functions, most of which maintain cellular redox homeostasis. A high level of reduction for glutathione (GSH, $1.0–10 \times 10^{-3}$ M) is one of the biochemical characteristics of a malignant tumor (Liu et al., 2016). Most recently, it was documented that the reduction–oxidation (redox) balance in tissue is regulated in part by the relative concentrations of reduced GSH and its oxidized disulfide counterpart that can influence gene expression, cellular differentiation, proliferation, and apoptosis (Burhans and Heintz, 2009). Thus, the modulatory role of metal complexes and their effect on GSH is also of importance in studying and exploring the probable mechanism of cell death or apoptosis. It has been reported that ternary metal(II) complexes exhibit significantly strong toxicity, and the diimine co-ligand plays a major part in inducing cell death (Rajendiran et al., 2008; Farrell, 2012; Yu et al., 2016). Some are lipophilic, thus resulting in greater cell uptake and higher toxicity (Maity et al., 2009; Ramakrishnan et al., 2009; Goswami et al., 2011).

Herein, we reported Cu(II) and Zn(II) complexes exhibiting a five-coordinated distorted square pyramidal geometry with solubility in water and DMSO (Scheme, Fig. 1). The primary objective of preparing these complexes is to evaluate their potential anticancer activity at varying concentrations after having sought out the most probable apoptotic mechanistic pathways by utilizing various *in vitro* cytotoxicity assays. Cell cycle and apoptotic assays were also carried out to assess the mechanism underlying the induction of cell death and ascertain the chemotherapeutic potential of these complexes.

2. Experimental

2.1. Materials and instrumentation

All chemicals and solvents were purchased from Sigma-Aldrich, Alfa Aesar, and Fluka, and used without further purification. All the consumables were procured from Nunc.

Absorption spectra were examined on a Thermo Scientific Evolution 201 spectrophotometer (200 to 1000 nm). Elemental analysis (CHN) was conducted on a Perkin Elmer 2400 Series II CHNS/O system (samples dried in vacuo to constant weight (25 °C, ca. 0.1 Torr). A Shimadzu IR Affinity-1 spectrophotometer was employed for obtaining infrared spectra (4000 to 400 cm^{-1}). NMR was recorded on a JEOL-ECP 400 system with the DMSO d_6 solvent (400 MHz for ^{1}H, 100 MHz for ^{13}C). Mass spectra was analyzed on a DART-TOF-MS mass spectrometer. The auto magnetic susceptibility balance from Sherwood Scientific Ltd. Molar conductance was determined on a Eutech Con510.

2.2. Synthesis

2.2.1. Synthesis of [Cu(tryp)(Hnor)₂(DMSO)]NO₃ (1)

Complex **1** was prepared by following the general synthetic method; tryptophan (204 mg, 1.0 mmol) was treated with KOH (56 mg, 1.0 mmol) for 30 min in methanol (20 cm³) at 298 K, which yielded a clear solution. To this solution, Cu(NO₃)·3H₂O (241 mg,
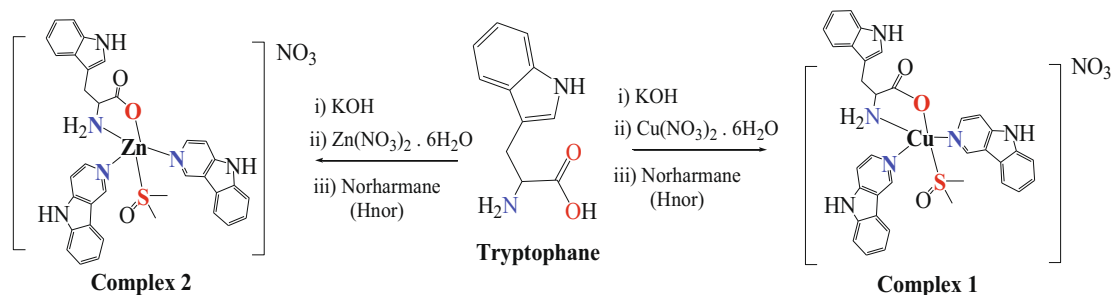
Fig. 1. Schematic representation of the synthesis of the two ternary complexes: [Cu(tryp)(Hnor)$_2$(DMSO)]NO$_3$ **(1)** and [Zn(tryp)(Hnor)$_2$(DMSO)]NO$_3$ **(2)**.

1.0 mmol) in a mixture of methanol and DMSO (9 cm^3: 1 cm^3) was added; the solution was stirred for 1 h. Next, Hnor (336 mg, 2.0 mmol) was added to 10 cm^3 methanol dropwise, and stirring was carried out for 4 h at 343 K. After completion, the reaction mixture was filtered and left for slow evaporation. A dark green color crystalline product was isolated after 1 week, washed with hexane, chloroform, and methanol, and dried under vacuum. Yield = 78%. M.P. = 188–190 °C. Elemental analysis for C$_{35}$H$_{33}$CuN$_6$O$_3$S· NO$_3$ (%): Calculated C, 56.56; H, 4.47; N, 13.19; and S, 4.31. Found C, 56.49; H, 4.46; N, 13.16; and S, 4.29. FT-IR (KBr)/cm^{-1}: 3414 (br), 3291 (br), 3110 (br), 1626 (vs), 1559 (m), 1498 (m), 1447 (s), 1384 (s, NO$_3^-$), 1331 (s), 1243 (s), 1146 (m, S-DMSO), 1035 (m), 827 (m), 734 (s), 597 (m), and 422 (m). Mass for [Cu (tryp)(Hnor)$_2$(DMSO)–1H$^+$] or [C$_{35}$H$_{33}$CuN$_6$O$_3$S–1H$^+$] (+ve, DMSO, *m/z*): 679.21 (observed), 679.17 (expected) for [C$_{35}$H$_{33}$CuN$_6$O$_3$S–H$^+$]. Uv–Vis in DMSO, λ_{max}/nm at 298 K: 303, 337, 355, and 645. Molar conductance (Ω^{-1}cm^2 mol^{-1}) in DMSO at 298 K = 43. μ_{eff} = 1.89 μ_B at 298 K.

2.2.2. Synthesis of [Zn(tryp)(Hnor)$_2$(DMSO)]NO$_3$ (2)

Complex **2** was synthesized following a similar procedure as that adopted for **1**. Yield = 67%. M.P. = 213–214 °C. Elemental analysis for C$_{35}$H$_{33}$ZnN$_6$O$_3$S· NO$_3$ (%): Calculated C, 56.42; H, 4.46; N, 13.16; and S, 4.30. Found C, 56.35; H, 4.45; N, 13.09; and S, 4.27. FT-IR (KBr)/cm^{-1}: 3396 (br), 3290 (br) 3120 (br), 1625 (vs), 1558 (m), 1498 (m), 1446 (s), 1380 (s, NO$_3^-$), 1331(s), 1241 (s), 1146 (m, S-DMSO), 1034 (m), 827 (m), 733 (s), 599 (m), and 430 (m). ^{1}H NMR (400 MHz, DMSO d_6,δ, ppm): 11.72 (s, 2 N-H of Hnor); 10.94 (s, 1 N-H of tryp); 8.92 (s, 4H of Hnor); 8.33 (d, 4H of Hnor, *J* = 5.2 Hz); 8.23 (d, 4H of Hnor, *J* = 8.0 Hz); 8.10 (d, 4H of Hnor, *J* = 5.2 Hz); 7.63 (m, 9H, 8H of Hnor and 1H of tryp, *J* = Hz); 7.63 (m, 5H, 4H of Hnor and 2H of tryp); 7.03–6.99 (t, 1H of tryp, *J* = 7.2 Hz); 6.92–6.88 (t, 1H of tryp, *J* = 7.2 Hz); 3.42 (s, br, 9H, 6H-CH$_3$ of DMSO, 2H of NH$_2$ and 1H of C-H tryp); and 2.49–2.48 (d, 2H of tryp, *J* = 1.6 Hz). ^{13}C NMR (100 MHz, DMSO d_6, δ, ppm): 157.13 (C = O), 140.69, 137.55, 135.91, 134.09, 128.35, 127.34, 122.03, 120.58, 119.38, 118.36, 114.68, 111.81, 91.00, 76.07, 39.50 (S-DMSO), and 27.91. MW for [Zn(tryp)(Hnor)$_2$(DMSO)–H$^+$] or [C$_{35}$H$_{33}$ZnN$_6$O$_3$S–H$^+$] (+ve, DMSO, *m/z*): 680.08 (observed), 680.16 (expected) for [C$_{35}$H$_{33}$CuN$_6$O$_3$S–H$^+$]. Uv–Vis in DMSO, λ_{max}/nm at 298 K: 304, 336, and 356. Molar conductance (Ω^{-1}cm^2 mol^{-1}) in DMSO at 298 K = 39.

2.3. Computational methodology

The full geometry optimization, single-point energy and vibrational frequency analysis, and time-dependent density functional theory (TD-DFT) calculations were carried out at the DFT level of theory using the B3LYP function (Lee et al., 1988; Becke, 1993; Stephens et al., 1994) with the help of the Gaussian-09 program package (Frisch et al., xxxx). The calculations were performed using 6-31G* basis sets (Hay and Wadt, 1985) for C, H, N, O, and

S atoms, and typical effective core potential (ECP) basis LanL2DZ (Los Alamos National Laboratory 2 double ζ) as an extra basis set (Wadt and Hay, 1985; Roy et al., 2008) for Cu and Zn atoms. All DFT calculations were performed without counter ions by employing the polarizable continuum model, 'CPCM' (DMSO as a solvent) (Draper and Hadley, 1990; Barone and Cossi, 1998; Cossi et al., 2003). No symmetry restrictions were applied during geometry optimization. The Hessian matrix was calculated analytically for the optimized structures to prove the location of the correct minima (no imaginary frequencies). The Cartesian atomic coordinates of the calculated optimized structures in DMSO are given in the ESI material.

2.4. In vitro cytotoxicity

All experiments were conducted using standard protocols with slight modifications adopted by us (Buege and Aust, 1978; Chandra et al., 2002; Siddiqui et al., 2010; Siddiqui et al., 2013; Khan et al., 2014; Yousuf et al., 2015). The cell cultures of HepG2 and MCF7 cancer cell lines were cultured in DMEM and maintained at 37 °C. The MTT assay was performed and read at 550 nm and IC$_{50}$ values were evaluated. Morphological images were taken on the phase-contrast microscope at 20 × magnification. The generation of ROS was assessed by DCFH-DA dye as per the protocol and images were taken using the fluorescence microscope. The intracellular GSH depletion was carried out by the Chandra et al. protocol (Sears et al., 1956) and the absorbance was read at 412 nm. The lipid peroxidation (LPO) assay was performed using the TBARS protocol and the absorbance of the supernatant was read at 550 nm. The apoptosis and cell cycle arrest studies were conducted using the standard protocol with the help of the available kits (Annexin V-FITC Apoptosis Detection kit, BD Biosciences) using flow cytometry.

3. Results and discussion

3.1. Synthesis and characterization

Ternary Cu(II)/Zn(II) complexes viz, [Cu(tryp)(Hnor)$_2$(DMSO)] NO$_3$ **(1)** and [Zn(tryp)(Hnor)$_2$(DMSO)]NO$_3$ **(2),** containing tryp and Hnor, were prepared in significantly robust yield and characterized by analytical and various spectroscopic techniques. Both **1** and **2** were 1:1 electrolyte in nature (39–43 Λ_M/S m^2 mol^{-1}) (Patra et al., 2008), while also being found soluble in DMSO and partially soluble in H$_2$O. They exhibited strong charge-transfer bands near 335 and 355 nm, respectively and **1** displayed a d-d transition ~ 645 nm in DMSO (see SI for Figure S1 and S2). Further, **1** and **2** are considerably stable toward air and moisture for >24 h. The structures of **1** and **2** exhibited distorted square pyramidal geometry, which is similar to what the literature reported previously (Khan et al., 2016) and the analytical data are found to be consistent with the proposed molecular formulae **(Scheme in** Fig. 1**)**.

The FT-IR spectra of **1** and **2** exhibited N-H bands at ~ 3400 cm^{-1} for the Hnor ligands. (Calligaris and Carugo, 1996) described characteristics of tryp's coordinated NH$_2$ bands around 3290 cm^{-1} and carboxylate (-O-C = O) bands ~ 1625 cm^{-1}, which showed a significant shift from the free tryp ~ 1660 cm^{-1} (Khan et al., 2016). The antisymmetric and symmetric -C = O stretching vibration shifted to lower frequencies that confirms the terminal coordination mode of carboxylate. The signal at ~ 1384 cm^{-1} marked the presence of uncoordinated NO$_3^-$ anion. Additionally, the peak associated with the S coordinated DMSO was observed at 1146 cm^{-1} (Calligaris, 2004; Arjmand et al., 2010). The coordination with the metal centers, i.e., Cu(II) and Zn(II), was confirmed by the M−O and M−N peaks at 597–599 and 430–422 cm^{-1}, respectively (see SI for Figure S2).

The ^{1}H NMR spectrum of the [Zn(tryp)(Hnor)$_2$(DMSO)]NO$_3$ **(2)** in DMSO d_6 exhibited all the characteristic signals associated with the proposed structure (see SI for Figure S3-S5). The signal at 11.72 ppm is attributed to the Hnor ligands aromatic N-H protons. Meanwhile, the peak associated with the NH proton of tryp was assigned at 10.94 ppm. An 8.92 ppm singlet as well as doublets at 8.33, 8.23, and 8.10 were associated with the Hnor protons. Two multiplets were observed comprised of aromatic protons at 7.63 and 7.36 ppm for both tryp and Hnor. Further, two triplets at 7.03 and 6.93 ppm were assigned to tryp. The multiplet at 3.42 ppm was attributed to signals of DMSO and tryp's NH$_2$. The ^{13}C NMR spectrum of [Zn(tryp)(Hnor)$_2$(DMSO)]NO$_3$ **(2)** in DMSO d_6 was responsible for the signal at 157 ppm associated with the C = O of tryp. The aromatic signals lying from 140.69 to 91.00 ppm and the aliphatic carbons at 76.07, 39.50, and 27.91 ppm were allied with tryp and the S-coordinated DMSO.

3.2. Computational chemistry

Density function theory (DFT) calculations were performed to investigate geometric and electronic features as the crystal structures of complexes not yet determined. The proposed structure has been optimized at the B3LYP level of DFT theory. The optimized structures of both complexes are shown in Fig. 2, indicating the geometry around the d^9 Cu(II) and d^{10} Zn(II) ion are found to be distorted square pyramidal with the two donor N atoms of the Hnor ligand and one N and one O donor atom of the tryp moiety while the axial coordination site was completed by the O atom of the DMSO molecule. The calculated bond lengths are given in Table S1 and are in robust agreement with the previously reported single-crystal X-ray data in various publications. The vibrational spectra have also been simulated to validate the proposed structure of complexes (see SI for Figure S6). The calculated frequencies and other spectral features were found within the range as shown

in Table S2. Two factors could be responsible for the deviation in the computed spectra: 1) an environmental factor, such as DFT calculations, were performed with solvation effects (liquid phase) while experimental data were obtained in the solid state; 2) the calculated frequencies only contained harmonic effects while experimental frequencies have both harmonic and anharmonic effects; and 3) basis set discrepancies. However, the pattern and trend of spectra were quite similar in both cases, thereby validating the proposed structures for complexes. Moreover, we calculated the UV–vis spectra to further support the calculated geometry of the complexes (see SI for Figure S7). The TD-DFT calculations were performed with DMSO for its solvation effects with both complexes. The significant features of the calculated UV–vis spectra strongly match the experimental spectra. Interestingly, the experimentally observed band within the ~ 645 nm range was also observed in the TD-DFT calculated spectrum, though it is absent in **2**, alternatively validating the proposed molecular geometry of both complexes.

The literature reveals that the HOMO and LUMO energy parameters could be related to the biological activities of the molecules. A small energy gap (ΔE) between the HOMO and LUMO indicates a more polarizable behavior of molecules and acts as a soft molecule with higher chemical and biological activity. However, molecules with a greater energy gap offer enhanced stability and lower activity than those with smaller HOMO-LUMO energy gaps. The HOMOs of **1** and **2** were localized on the tryp moiety while the LUMOs were for the Hnor ligand. Interestingly, the HOMO-LUMO energy gap of **1** (0.10 eV) is smaller than **2** (0.29 eV), suggesting that **1** could show more significant biological activity compared to **2** (Fig. 3).

3.3. Anticancer activity

3.3.1. Cell viability

The assessment of the toxicity of **1** and **2** was carried out against two cancer cell lines, HepG2 (human liver hepatocellular carcinoma cells) and MCF7 (human breast cancer cells), and one non-tumorigenic HEK293 (human embryonic kidney) cells using the MTT assay. Cisplatin (standard drug) was used as a positive control and compared with the earlier reported similar compounds **(see Table 1)**. The IC$_{50}$ values exhibited the promising potential of **1**. The IC$_{50}$ value exhibited by **1** was ~ 10 ± 1.3 µM against MCF7 (breast cancer) cells. The IC$_{50}$ value against HepG2 was non-significant (~27 ± 1.1 µM). When **1** was compared to the standard drug, cisplatin, it showed significant toxicity and selectivity towards cancer cells and low toxicity towards non-cancerous cells (HEK293 cells, IC$_{50}$ value > 100 µM), which was also an encouraging finding.
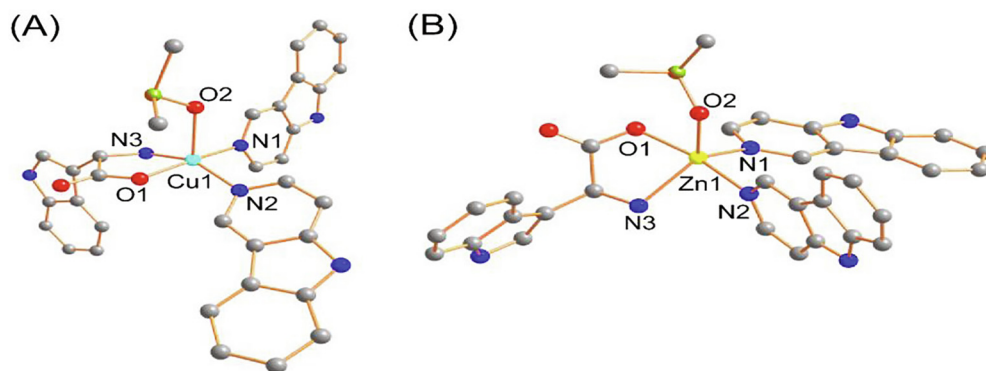

Fig. 2. DFT-optimized structures of (A) **1** and (B) **2**. Only coordinated donor atoms are labeled. H atoms are omitted for clarity.
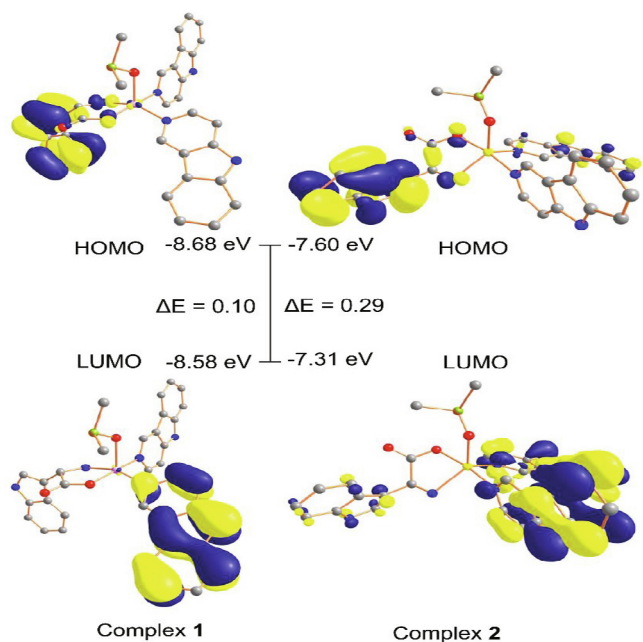
Fig. 3. Frontier molecular orbitals of **1** (left) and **2** (right) and their HOMO-LUMO energy gaps.

3.3.2. Cell morphology

The morphology of the MCF7 breast cancer cells with respect to treatment with **1** and **2** was investigated using a phase-contrast inverted microscope. The MCF7 cells prominently exhibited morphological changes upon exposure to **1**, where a significant reduction in cell adhesion capacity was observed compared with control along with a loss of its normal characteristics. This selectivity can be attributed to Hnor, possessing blood–brain barrier-crossing capability, the active aromatic rings of tryp and the high electron density of the Cu(II) ion, which facilitates the penetration of the molecules into the cell and may enable interaction with biomolecules, such as DNA and HSA (Chandra et al., 2002). This motivated us to go further in detail. Thus, **1** was selected to study the MCF7 breast cancer cell line in detail (Fig. 4).

3.3.3. Cell cycle arrest and apoptosis induced by complex 1 against MCF7 cells

It is well-known that the proliferation of cancer cells is inhibited by anticancer compounds through the induction of cell cycle arrest and/or apoptosis (Barbosa et al., 2018; Kumar et al., 2018; Fei et al., 2019). To study the growth inhibition mechanism of the MCF7 human breast cancer cell line by **1**, a cell cycle arrest kit was utilized for measuring the distribution of the cell phases through propidium iodide (PI) staining with flow cytometry (Fig. 5). There was a slight deviation of a population in the G1

and S phases from the control, but cells in the G2 and M phases were notably diminished in the fraction. This led us to pronounce the G2/M phase of cell cycle is arrested by **1**.

Further, we employed the Annexin V-FITC Apoptosis Detection kit using flow cytometry to further establish the ability of **1** in MCF7 breast cancer cells to induce apoptosis. The cancer cells are known to divide relentlessly and, owing to a lack of apoptosis, survive (Kumar et al., 2018) with various metal complexes known to be implicated in this apoptotic pathway (Marzano et al., 2009; Kowol et al., 2012). Thus, MCF7 cancer cells were treated with **1** at three concentrations—7, 10, and 15 μM. It can be seen in Fig. 6 that there was a concentration-dependent apoptotic pathway pursuit with **1**. At lower concentrations than the IC$_{50}$ value (7 μM), apoptosis was observed at 7.3% and early apoptosis at 31.2% upon moving to the higher concentration (10 μM), with the percentage of apoptosis rising to 27.7% (apoptotic cells). There was a further increase when moving to a concentration greater than the IC$_{50}$ value (15 μM), and the number of apoptotic cells rose to 37.1%. Similarly, a rise in necrosis was also observed. However, the data suggested a predominance of the apoptotic pathway being stimulated with the toxicity of **1** acting in MCF7 cancer cells (Fig. 6).

3.3.4. ROS generation

Cu-based anticancer drugs are known to generate ROS, hydroxyl radicals (OH$^\bullet$), singlet O radicals ($^1O_2^\bullet$), and superoxide radicals ($O_2^{\bullet-}$), which are responsible for their potential in acting as anticancer drugs. The production of ROS is Cu-driven, regardless of the oxidation state of Cu, i.e., Cu$^+$/Cu^{2+}, that enters the body. Cu$^+$ ions reduce H$_2$O$_2$ and produces OH$^\bullet$, whereas Cu^{2+} ions reduce to Cu$^+$ ions by O$_2^{\bullet-}$ or GSH (Gomes et al., 2005; Tisato et al., 2010). Excess of intracellular ROS can lead to DNA damage and trigger the p53 gene along with various other genes. Therefore, ROS generation by **1** in MCF7 human breast cancer cells was estimated by an FL-based assay using the dye, 2,7-dichlorofluorescein diacetate (DCFH-DA) (Wang and Joseph, 1999; Shao et al., 2014; Prosser et al., 2017). Upon treatment of MCF7 cells with **1**; a significant increase in ROS was noted from Fig. 7. Thus, the elevation of ROS in MCF7 cells ascertains the oxidative DNA damage as a possible mode of action, which is consistent with the earlier reported literature (Fig. 7) (Zimmermann and Burda, 2010).

3.3.5. Intracellular GSH and LPO levels in MCF7 cells

In the human body, the most abundant thiol-containing compound is GSH. It is a tripeptide, γ-Glu-Cys-Gly which is present in biological fluids ubiquitously at a 1–10 mM concentration (Kreżel and Bal, 1999; Florea and Büsselberg, 2011; Cadoni et al., 2017). The two GSH molecules bonded through a disulfide bridge, GSSG, which is formed by their oxidized form and thus exists in equilibrium. When the ratio of GSH/GSSG is reduced to less than 10, the depletion of GSH is often associated with cancer emerging (Cotgreave et al., 1988; Ortega et al., 2011). Reduced/oxidized GSH has the potential to create a complex with Cu. The flow diagram of Fig. 8 represents the antioxidant mode of GSH and the superoxide

Table 1
The cell viability assay (MTT assay) lists IC$_{50}$ values (in μM) for the treatment of two human cancer cell lines and a non-tumorigenic cell line.

Complex	HepG2(μM)	MCF7(μM)	HEK293 (μM)	[Ref]
[Cu(tryp)(Hnor)$_2$(DMSO)]NO$_3$ **(1)**	27 ± 1.1	10 ± 1.3	>100	
[Zn(tryp)(Hnor)$_2$(DMSO)]NO$_3$ **(2)**	88 ± 1.9	24 ± 1.7	>150	
[Cu(tryp)1,2-diaminobenzene] Cl	ND	less than10	ND	(Chen et al., 2016)
[Zn(tryp)1,2-diaminobenzene] Cl	ND	35	ND	(Chen et al., 2016)
Cu(NO$_3$)$_2$	>200	>200	>200	
Zn(NO$_3$)$_2$	>200	>200	>200	
Free Hnor	>200	>200	>200	
Free tryp	>200	>200	>200	
Cisplatin	7.63 ± 1.6	38 ± 1.23	>50	(Karmakar et al., 2016; Xu et al., 2017)
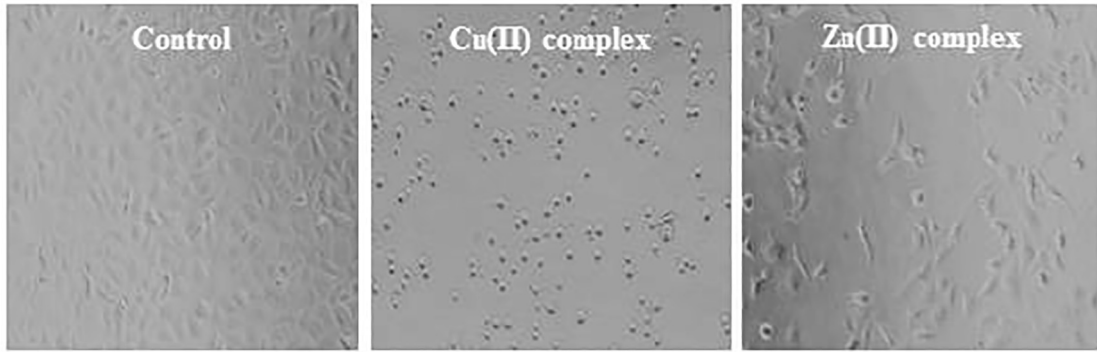
Fig. 4. Morphological changes of MCF7 cells induced by **1** and **2** at a concentration of 10 μM.
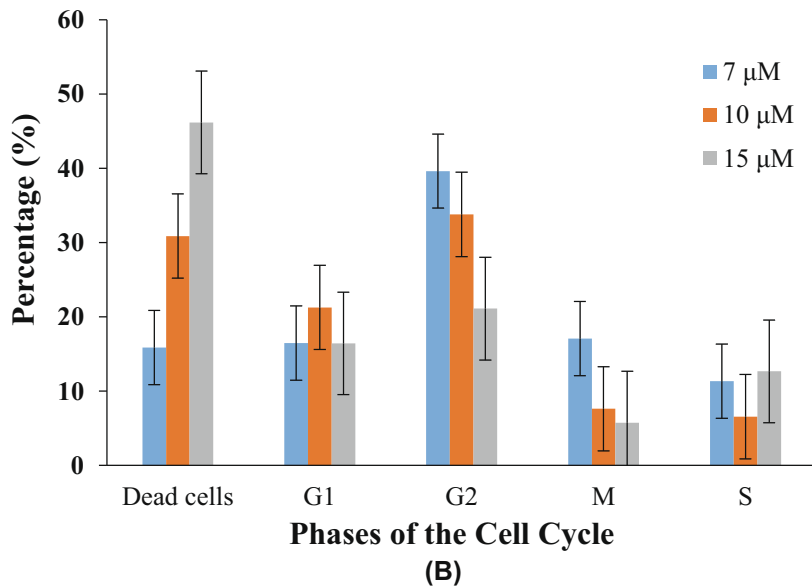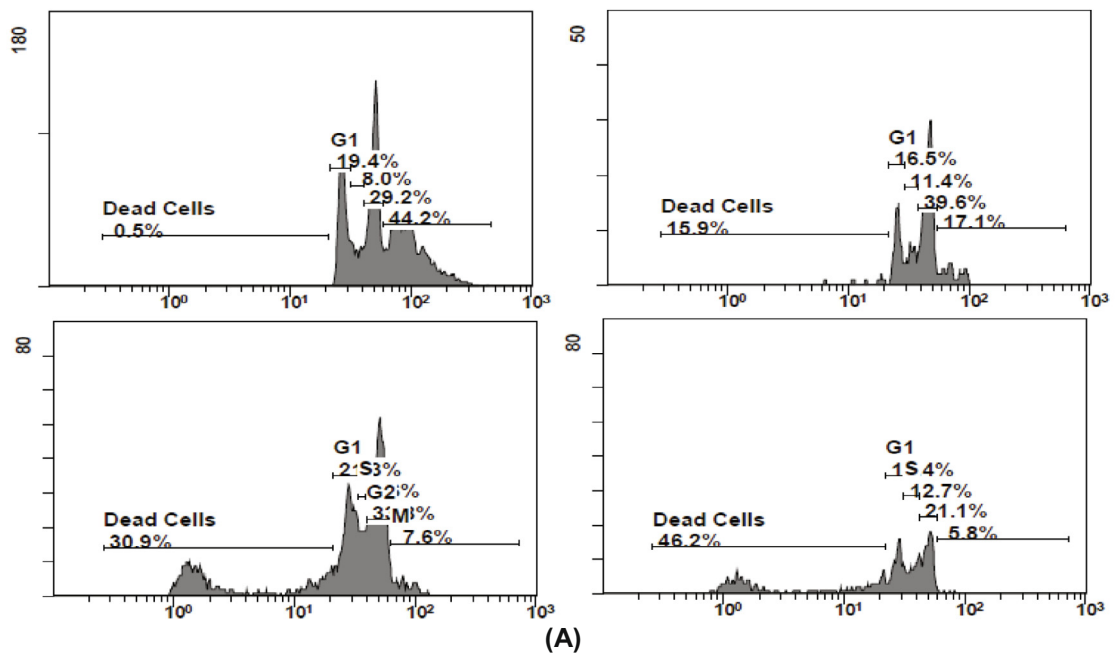

(A)

(B)

Fig. 5. Cell cycle analysis determined (A) cell populations in each phase and (B) a histogram showing the treated cells with different concentrations of **1** in each phase within MCF7 cancer cells.
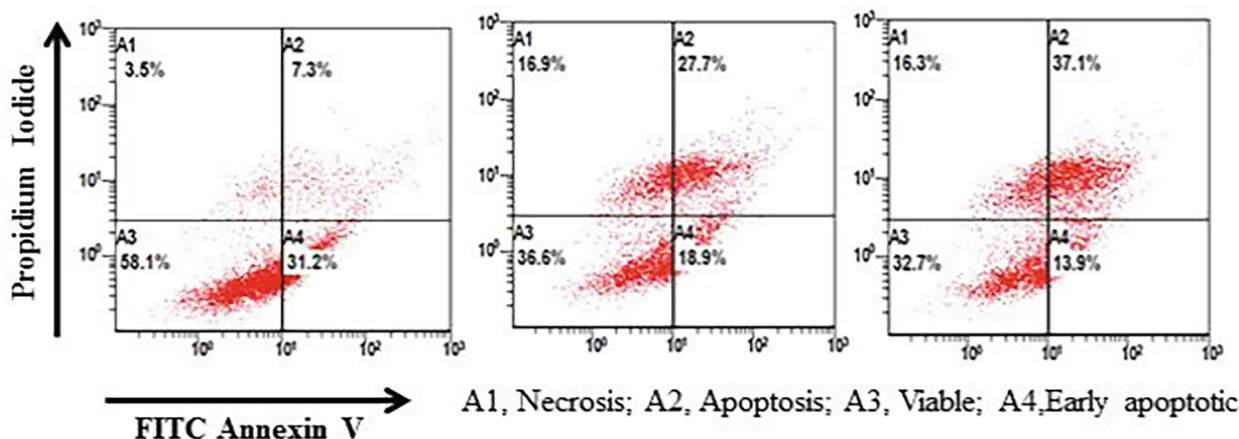
Fig. 6. Flow cytometry analysis of apoptotic induction by **1** in the MCF7 cell line at a concentration of 7, 10, and 15 μM using an Annexin V-FITC Apoptosis Detection kit.
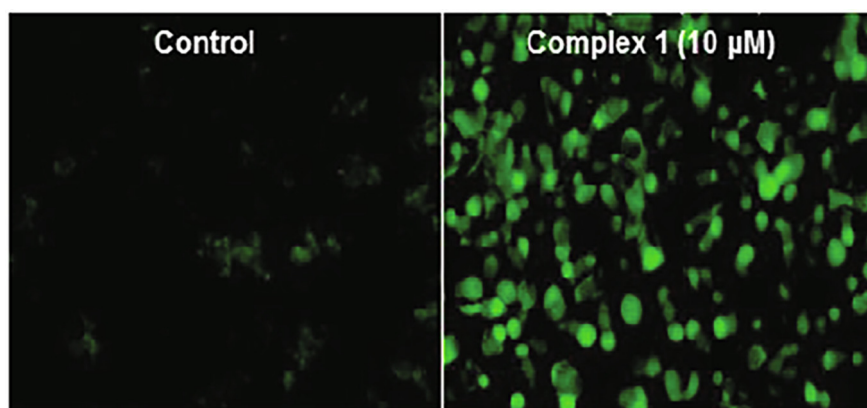

Fig. 7. ROS generation in MCF7 cells exposed to **1** at a concentration of 10 μM.

dismutase induced by Cu(II)-disulfide (RSSR) (Fig. 8(i)). To examine the role of oxidative stress with respect to cytotoxicity, the effect of **1** was evaluated based on intracellular GSH levels. It is known that the GSH/GSSG ratio affects cell cycle regulation, synthesis of DNA, mutagenic pathways, drug resistance, etc. in cancer cells. Typically, cancer cells possess a higher level of GSH compared to normal cells (Cotgreave et al., 1988; Masella et al., 2005). Therefore, we investigated the levels of GSH in MCF7 human breast cancer cells treated with **1** (Fig. 8). The histogram represents the depletion of GSH in a concentration-dependent manner. This significant reduction in GSH levels (>55%) reveals the role of oxidative stress in cytotoxicity (Fig. 8(ii)).

It is well-known that LPO caused by oxidative damage to lipids leads to upsetting the integrity of the cell membranes and organelles, like mitochondria. LPO is thermodynamically as well as kinetically favored, i.e., lipid reacts swiftly to $HO_2^.$ (peroxyl radicals) whereas lipid radicals react to $O_2^{.-}$ (superoxide radical). Thus, we assessed LPO in MCF7 cancer cells treated with **1**. The results indicated elevation of LPO levels to > 50%. These results indicated to us stimulation of the oxidative pathway, in which GSH levels decrease and LPO levels rise, supporting the redox changes prompted by **1** and leading to damage and death to the cells.

4. Conclusion

In summary, we have designed and synthesized new ternary metal complexes with biocompatible β-carboline Hnor and tryp, [Cu(tryp)(Hnor)$_2$(DMSO)]NO$_3$ **1** and [Zn(tryp)(Hnor)$_2$(DMSO)]NO$_3$ **2**, and characterized them with various experimental techniques and theoretically validated by computational studies. To study the chemotherapeutic potential of the two complexes as anticancer agents, *in vitro* treatment on two cancer cell lines, HepG2 and MCF7, and one non-tumorigenic, HEK293 cell lines were assessed. The MTT assay determined the substantial selective potential of **1** against MCF7 cancer cells when compared to cisplatin (standard drug). Furthermore, the mechanistic pathway evaluation confirmed G2/M phase cell population arrest, primarily because of apoptotic pathways being activated. ROS generation, LPO elevation, and GSH depletion was observed and confirmed the presence of redox potential changes associated with **1** inside the MCF7 cells. The apoptotic pathway is a key mechanism by which cancer cells are eliminated by cytotoxic drugs. Activation of apoptotic pathways can be intrinsic (mitochondrial) or extrinsic (cytoplasmic) and its understanding has served as the basis of novel targeted therapies. The selective behavior of **1** toward tumor cells compared to non-tumorigenic cells render the potential molecule candidate a preferentially selective chemotherapeutic agent against human breast cancer and merits further investigation in detail, possibly paving the way for future therapeutic design and interventions.
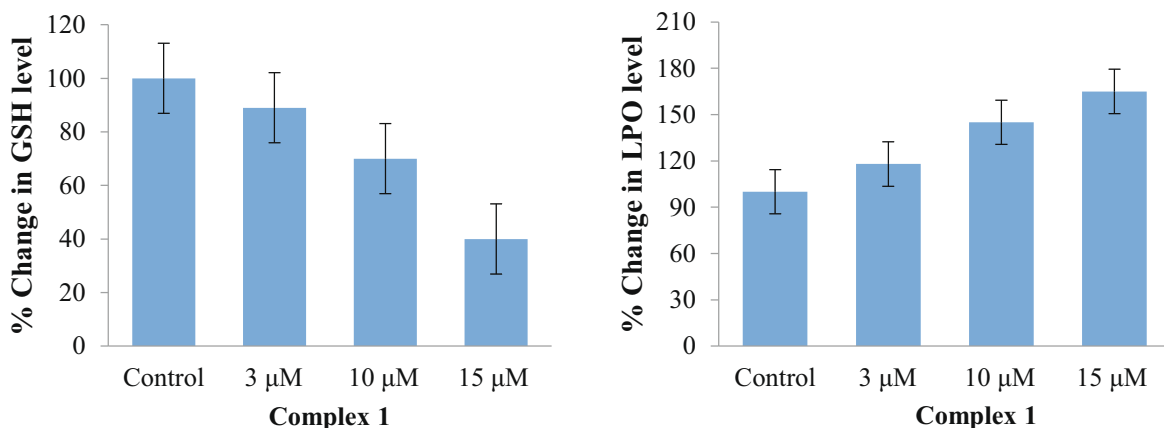
(i)
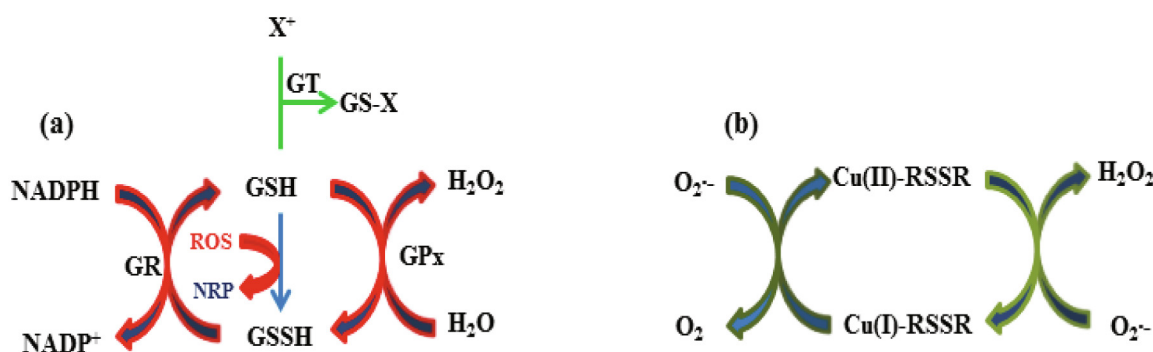
(ii)

Fig. 8. (i) The concentration-dependent activity of **1** exhibited by the percent change in LPO and GSH in the MCF7 cell line. **(ii)** The possible mechanism associated with (a) anti-oxidant action of GSH and (b) dismutation of superoxide induced by the Cu(II)-RSSR complex (GR, glutathione reductase; GPx, glutathione peroxidase; NRP, non-radical product; X^+, pro-oxidant electrophile).

Appendix A. Supplementary material

Supplementary data to this article can be found online at https://doi.org/10.1016/j.sjbs.2020.05.001.

References

Alsalme, A., Khan, R.A., Alkathiri, A.M., Ali, M., Tabassum, S., Jaafar, M. and Al-Lohedan, H.A., 2018. β-Carboline Silver Compound Binding Studies with Human Serum Albumin: A Comprehensive Multispectroscopic Analysis and Molecular Modeling Study. Bioinorganic Chemistry and Applications, 2018.

Arjmand, F., Muddassir, M., Khan, R.H., 2010. Chiral preference of l-tryptophan derived metal-based antitumor agent of late 3d-metal ions (Co (II), Cu (II) and Zn (II)) in comparison to d-and dl-tryptophan analogues: Their in vitro reactivity towards CT DNA, 5′-GMP and 5′-TMP. Eur. J. Med. Chem. 45 (9), 3549–3557. https://doi.org/10.1016/j.ejmech.2010.04.031.

Barbosa, F.A., Siminski, T., Canto, R.F., Almeida, G.M., Mota, N.S., Ourique, F., Pedrosa, R.C., Braga, A.L., 2018. Novel pyrimidinic selenourea induces DNA damage, cell cycle arrest, and apoptosis in human breast carcinoma. Eur. J. Med. Chem. 155, 503–515. https://doi.org/10.1016/j.ejmech.2018.06.026.

Barone, V., Cossi, M., 1998. Quantum calculation of molecular energies and energy gradients in solution by a conductor solvent model. J. Phys. Chem. A 102 (11), 1995–2001.

Becke, A.D., Density-functional thermochemistry. III. The role of exact exchange (1993) Journal of Chemical Physics, 98, p. 5648.

Bruijnincx, P.C., Sadler, P.J., 2008. New trends for metal complexes with anticancer activity. Curr. Opin. Chem. Biol. 12 (2), 197–206.

Buege, J.A., Aust, S.D., 1978. [30] Microsomal lipid peroxidation. In: Methods in Enzymology. Academic Press, pp. 302–310.

Burhans, W.C., Heintz, N.H., 2009. The cell cycle is a redox cycle: linking phase-specific targets to cell fate. Free Radical Biol. Med. 47 (9), 1282–1293. https://doi.org/10.1016/j.freeradbiomed.2009.05.026.

Cadoni, E., Valletta, E., Caddeo, G., Isaia, F., Cabiddu, M.G., Vascellari, S., Pivetta, T., 2017. Competitive reactions among glutathione, cisplatin and copper-phenanthroline complexes. J. Inorg. Biochem. 173, 126–133.

Calligaris, M., 2004. Structure and bonding in metal sulfoxide complexes: an update. Coord. Chem. Rev. 248 (3–4), 351–375. https://doi.org/10.1016/j.ccr.2004.02.005.

Calligaris, M., Carugo, O., 1996. Structure and bonding in metal sulfoxide complexes. Coord. Chem. Rev. 153, 83–154. https://doi.org/10.1016/0010-8545(95)01193-5.

Chandra, D., Ramana, K.V., Wang, L., Christensen, B.N., Bhatnagar, A., Srivastava, S.K., 2002. Inhibition of fiber cell globulization and hyperglycemia-induced lens opacification by aminopeptidase inhibitor bestatin. Invest. Ophthalmol. Vis. Sci. 43 (7), 2285–2292.

Chen, D., Cui, Q.C., Yang, H., Dou, Q.P., 2006. Disulfiram, a clinically used anti-alcoholism drug and copper-binding agent, induces apoptotic cell death in breast cancer cultures and xenografts via inhibition of the proteasome activity. Cancer Res. 66 (21), 10425–10433.

Chen, L.M., Peng, F., Li, G.D., Jie, X.M., Cai, K.R., Cai, C., Zhong, Y., Zeng, H., Li, W., Zhang, Z., Chen, J.C., 2016. The studies on the cytotoxicity in vitro, cellular uptake, cell cycle arrest and apoptosis-inducing properties of ruthenium methylimidazole complex [Ru (MeIm) 4 (p-cpip)] 2+. J. Inorg. Biochem. 156, 64–74. https://doi.org/10.1016/j.jinorgbio.2015.12.016.

Cossi, M., Rega, N., Scalmani, G., Barone, V., 2003. Energies, structures, and electronic properties of molecules in solution with the C-PCM solvation model. J. Comput. Chem. 24 (6), 669–681.

Cotgreave, I.A., Moldeus, P., Orrenius, S., 1988. Host biochemical defense mechanisms against prooxidants. Annu. Rev. Pharmacol. Toxicol. 28 (1), 189–212. https://doi.org/10.1146/annurev.pa.28.040188.001201.

Creaven, B.S., Czeglédi, E., Devereux, M., Enyedy, É.A., Kia, A.F.A., Karcz, D., Kellett, A., McClean, S., Nagy, N.V., Noble, A., Rockenbauer, A., 2010. Biological activity and coordination modes of copper (II) complexes of Schiff base-derived coumarin ligands. Dalton Trans. 39 (45), 10854–10865.

Draper, H.H., Hadley, M., 1990. [43] Malondialdehyde determination as index of lipid Peroxidation. In: Methods in enzymology. Academic press, pp. 421–431. 10.1016/0076-6879(90)86135-i.

Farrell, N., 2012. Transition metal complexes as drugs and chemotherapeutic agents. Springer Science & Business Media.

Fei, B.L., Tu, S., Wei, Z., Wang, P., Qiao, C., Chen, Z.F., 2019. Optically pure chiral copper (II) complexes of rosin derivative as attractive anticancer agents with potential anti-metastatic and anti-angiogenic activities. Eur. J. Med. Chem. 176, 175–186.

Festa, R.A., Thiele, D.J., 2011. Copper: an essential metal in biology. Curr. Biol. 21 (21), R877–R883.

Filipović, N.R., Bjelogrlić, S., Marinković, A., Verbić, T.Ž., Cvijetić, I.N., Senćanski, M., Rodić, M., Vujčić, M., Sladić, D., Striković, Z., Todorović, T.R., 2015. Zn (II) complex with 2-quinolinecarboxaldehyde selenosemicarbazone: synthesis, structure, interaction studies with DNA/HSA, molecular docking and caspase-8 and-9 independent apoptose induction. RSC Adv. 5 (115), 95191–95211.

Florea, A.M., Büsselberg, D., 2011. Cisplatin as an anti-tumor drug: cellular mechanisms of activity, drug resistance and induced side effects. Cancers 3 (1), 1351–1371. https://doi.org/10.3390/cancers3011351.

Frisch, M.J. and MJ, G., Trucks, HB Schlegel, GE Scuseria, MA Robb, JR Cheeseman, G. Scalmani, V. Barone, B. Mennucci, GA Petersson and H. Nakatsuji, et al., Gaussian, 9.

Gomes, A., Fernandes, E., Lima, J.L., 2005. Fluorescence probes used for detection of reactive oxygen species. J. Biochem. Bioph. Methods 65 (2–3), 45–80. https://doi.org/10.1016/j.jbbm.2005.10.003.

Goswami, T.K., Chakravarthi, B.V., Roy, M., Karande, A.A., Chakravarty, A.R., 2011. Ferrocene-conjugated L-tryptophan copper (II) complexes of phenanthroline bases showing DNA photocleavage activity and cytotoxicity. Inorg. Chem. 50 (17), 8452–8464.

Hassouneh, B., Islam, M., Nagel, T., Pan, Q., Merajver, S.D., Teknos, T.N., 2007. Tetrathiomolybdate promotes tumor necrosis and prevents distant metastases by suppressing angiogenesis in head and neck cancer. Mol. Cancer Ther. 6 (3), 1039–1045.

Hay, P.J., Wadt, W.R., 1985. Ab initio effective core potentials for molecular calculations. Potentials for the transition metal atoms Sc to Hg. J. Chem. Phys. 82 (1), 270–283.

Huang, X., Liu, R., Li, J., Liang, X., Lan, Q., Shi, X., Pan, L., Chen, H., Ma, Z., 2019. Synthesis, characterization, anti-tumor activity, photo-luminescence and BHb/HHb/Hsp90 molecular docking of zinc (II) hydroxyl-terpyridine complexes. J. Inorg. Biochem. 201, 110790.

Kachadourian, R., Brechbuhl, H.M., Ruiz-Azuara, L., Gracia-Mora, I., Day, B.J., 2010. Casiopeína IIgly-induced oxidative stress and mitochondrial dysfunction in human lung cancer A549 and H157 cells. Toxicology 268 (3), 176–183. https://doi.org/10.1016/j.tox.2009.12.010.

Karmakar, S., Chatterjee, S., Purkait, K., Mukherjee, A., 2016. Anticancer activity of a chelating nitrogen mustard bearing tetrachloridoplatinum (IV) complex: better stability yet equipotent to the Pt (II) analogue. Dalton Trans. 45 (29), 11710–11722. https://doi.org/10.1039/C6DT00831C.

Khan, R.A., De Almeida, A., Al-Farhan, K., Alsalme, A., Casini, A., Ghazzali, M., Reedijk, J., 2016. Transition-metal norharmane compounds as possible cytotoxic agents: New insights based on a coordination chemistry perspective. J. Inorg. Biochem. 165, 128–135. https://doi.org/10.1016/j.jinorgbio.2016.07.001.

Khan, R.A., Dielmann, F., Liu, X., Hahn, F.E., Al-Farhan, K., Alsalme, A., Reedijk, J., 2016. Tetrahedrally coordinated luminescent copper (I) compounds containing halide, phosphane and norharmane ligands. Polyhedron 111, 173–178.

Khan, R.A., De Almeida, A., Al-Farhan, K., Alsalme, A., Casini, A., Ghazzali, M. and Reedijk, J., 2016. Transition-metal norharmane compounds as possible cytotoxic agents: New insights based on a coordination chemistry perspective. Journal of Inorganic Biochemistry, 165, pp.128-135.

Khan, R.A., Yadav, S., Hussain, Z., Arjmand, F., Tabassum, S., 2014. Carbohydrate linked organotin (IV) complexes as human topoisomerase Iα inhibitor and their antiproliferative effects against the human carcinoma cell line. Dalton Trans. 43 (6), 2534–2548. https://doi.org/10.1039/C3DT51973B.

Kowol, C.R., Heffeter, P., Miklos, W., Gille, L., Trondl, R., Cappellacci, L., Berger, W., Keppler, B.K., 2012. Mechanisms underlying reductant-induced reactive oxygen species formation by anticancer copper (II) compounds. J. Biol. Inorg. Chem. 17 (3), 409–423. https://doi.org/10.1007/s00775-011-0864-x.

Krężel, A., Bal, W., 1999. Coordination chemistry of glutathione. Acta Biochim. Pol. 46 (3), 567–580.

Kumar, R., Chauhan, A., Jha, S.K. and Kuanr, B.K., 2018. Localized cancer treatment by radio-frequency hyperthermia using magnetic nanoparticles immobilized on graphene oxide: from novel synthesis to in vitro studies. Journal of Materials Chemistry B, 6(33), pp. 5385-5399. DOI: 10.1039/C8TB01365A.

Kumar, R., Chauhan, A., Jha, S.K., Kuanr, B.K., 2018. Localized cancer treatment by radio-frequency hyperthermia using magnetic nanoparticles immobilized on graphene oxide: from novel synthesis to in vitro studies. J. Mater. Chem. B 6 (33), 5385–5399. https://doi.org/10.1021/jm201220n.

Lazou, M., Hatzidimitriou, A.G., Papadopoulos, A.N., Psomas, G., 2019. Zinc-oxaprozin compounds: Synthesis, structure and biological activity. J. Inorg. Biochem. 195, 101–110.

Lee, C., Yang, W., Parr, R.G., 1988. Development of the Colle-Salvetti correlation-energy formula into a functional of the electron density. Physical Review B 37 (2), 785.

Liu, T., Lai, L., Song, Z., Chen, T., 2016. A sequentially triggered nanosystem for precise drug delivery and simultaneous inhibition of cancer growth, migration,

and invasion. Adv. Funct. Mater. 26 (43), 7775–7790. https://doi.org/10.1002/adfm.201604206.

Maity, B., Roy, M., Saha, S., Chakravarty, A.R., 2009. Photoinduced DNA and protein cleavage activity of ferrocene-conjugated ternary copper (II) complexes. Organometallics 28 (5), 1495–1505.

Malarz, K., Zych, D., Kuczak, M., Musioł, R., Mrozek-Wilczkiewicz, A., 2020. Anticancer activity of 4′-phenyl-2, 2′: 6′, 2 ″-terpyridines–Behind the metal complexation. Eur. J. Med. Chem. 112039

Marzano, C., Pellei, M., Tisato, F., Santini, C., 2009. Copper complexes as anticancer agents. Anti-Cancer Agents in Medicinal. Chemistry (Formerly Current Medicinal Chemistry-Anti-Cancer Agents) 9 (2), 185–211.

Masella, R., Di Benedetto, R., Varì, R., Filesi, C., Giovannini, C., 2005. Novel mechanisms of natural antioxidant compounds in biological systems: involvement of glutathione and glutathione-related enzymes. The Journal of Nutritional Biochemistry 16 (10), 577–586. https://doi.org/10.1016/j.jnutbio.2005.05.013.

Mohanty, M., Banerjee, A., Biswal, S., Horn Jr, A., Schenk, G., Brzezinski, K., Sinn, E., Reuter, H., Dinda, R., 2020. Polynuclear zinc (II) complexes of thiosemicarbazone: Synthesis, X-ray structure and biological evaluation. J. Inorg. Biochem. 203, 110908.

Ndagi, U., Mhlongo, N., Soliman, M.E., 2017. Metal complexes in cancer therapy–an update from drug design perspective. Drug design, development and therapy 11, 599.

Ortega, A.L., Mena, S., Estrela, J.M., 2011. Glutathione in cancer cell death. Cancers 3 (1), 1285–1310. https://doi.org/10.3390/cancers3011285.

Panice, M.R., Lopes, S.M., Figueiredo, M.C., Ruiz, A.L.T.G., Foglio, M.A., Formagio, A.S. N., Sarragiotto, M.H. and e Melo, T.M.P., 2019. New 3-tetrazolyl-β-carbolines and β-carboline-3-carboxylates with anti-cancer activity. European Journal of Medicinal Chemistry, 179, pp. 123-132.

Patra, A.K., Bhowmick, T., Ramakumar, S., Nethaji, M., Chakravarty, A.R., 2008. DNA cleavage in red light promoted by copper (II) complexes of α-amino acids and photoactive phenanthroline bases. Dalton Trans. 48, 6966–6976. https://doi.org/10.1039/B802948B.

Prosser, K.E., Chang, S.W., Saraci, F., Le, P.H., Walsby, C.J., 2017. Anticancer copper pyridine benzimidazole complexes: ROS generation, biomolecule interactions, and cytotoxicity. J. Inorg. Biochem. 167, 89–99. https://doi.org/10.1016/j.jinorgbio.2016.11.006.

Rajendiran, V., Murali, M., Suresh, E., Palaniandavar, M., Periasamy, V.S., Akbarsha, M.A., 2008. Non-covalent DNA binding and cytotoxicity of certain mixed-ligand ruthenium (II) complexes of 2, 2′-dipyridylamine and diimines. Dalton Trans. 16, 2157–2170.

Ramakrishnan, S., Rajendiran, V., Palaniandavar, M., Periasamy, V.S., Srinag, B.S., Krishnamurthy, H., Akbarsha, M.A., 2009. Induction of cell death by ternary copper (II) complexes of L-tyrosine and diimines: role of coligands on DNA binding and cleavage and anticancer activity. Inorg. Chem. 48 (4), 1309–1322.

Redza-Dutordoir, M., Averill-Bates, D.A., 2016. Activation of apoptosis signalling pathways by reactive oxygen species. Biochimica et Biophysica Acta (BBA)-Molecular. Cell Res. 1863 (12), 2977–2992. https://doi.org/10.1016/j.bbamcr.2016.09.012.

Roy, L.E., Hay, P.J., Martin, R.L., 2008. Revised basis sets for the LANL effective core potentials. J. Chem. Theory Comput. 4 (7), 1029–1031.

Ruiz-Azuara, L. and E Bravo-Gomez, M., 2010. Copper compounds in cancer chemotherapy. Current Medicinal Chemistry, 17(31), pp. 3606-3615.

Santini, C., Pellei, M., Gandin, V., Porchia, M., Tisato, F., Marzano, C., 2014. Advances in copper complexes as anticancer agents. Chem. Rev. 114 (1), 815–862.

Sears, P.G., Lester, G.R., Dawson, L.R., 1956. A Study of the Conductance Behavior of Some Uni-univalent Electrolytes in Dimethyl Sulfoxide at 25°. The Journal of Physical Chemistry 60 (10), 1433–1436.

Shaharyar, M., Abdullah, M.M., Bakht, M.A., Majeed, J., 2010. Pyrazoline bearing benzimidazoles: search for anticancer agent. Eur. J. Med. Chem. 45 (1), 114–119. https://doi.org/10.1016/j.ejmech.2009.09.032.

Shao, J., Ma, Z.Y., Li, A., Liu, Y.H., Xie, C.Z., Qiang, Z.Y., Xu, J.Y., 2014. Thiosemicarbazone Cu (II) and Zn (II) complexes as potential anticancer agents: Syntheses, crystal structure, DNA cleavage, cytotoxicity and apoptosis induction activity. J. Inorg. Biochem. 136, 13–23. https://doi.org/10.1016/j.jinorgbio.2014.03.004.

Shi, X., Chen, Z., Wang, Y., Guo, Z., Wang, X., 2018. Hypotoxic copper complexes with potent anti-metastatic and anti-angiogenic activities against cancer cells. Dalton Trans. 47 (14), 5049–5054. https://doi.org/10.1039/C8DT00794B.

Siddiqui, M.A., Kashyap, M.P., Kumar, V., Al-Khedhairy, A.A., Musarrat, J., Pant, A.B., 2010. Protective potential of trans-resveratrol against 4-hydroxynonenal induced damage in PC12 cells. Toxicol. in Vitro 24 (6), 1592–1598. https://doi.org/10.1016/j.tiv.2010.06.008.

Siddiqui, M.A., Ahmad, J., Farshori, N.N., Saquib, Q., Jahan, S., Kashyap, M.P., Ahamed, M., Musarrat, J., Al-Khedhairy, A.A., 2013. Rotenone-induced oxidative stress and apoptosis in human liver HepG2 cells. Mol. Cell. Biochem. 384 (1–2), 59–69. https://doi.org/10.1007/s11010-013-1781-9.

Skrott, Z., Mistrik, M., Andersen, K.K., Friis, S., Majera, D., Gursky, J., Ozdian, T., Bartkova, J., Turi, Z., Moudry, P., Kraus, M., 2017. Alcohol-abuse drug disulfiram targets cancer via p97 segregase adaptor NPL4. Nature 552 (7684), 194–199.

Stefani, C., Al-Eisawi, Z., Jansson, P.J., Kalinowski, D.S., Richardson, D.R., 2015. Identification of differential anti-neoplastic activity of copper bis (thiosemicarbazones) that is mediated by intracellular reactive oxygen species generation and lysosomal membrane permeabilization. J. Inorg. Biochem. 152, 20–37.

Stephens, P.J., Devlin, F.J., Chabalowski, C.F.N., Frisch, M.J., 1994. Ab initio calculation of vibrational absorption and circular dichroism spectra using density functional force fields. The Journal of Physical Chemistry 98 (45), 11623–11627.

Tisato, F., Marzano, C., Porchia, M., Pellei, M., Santini, C., 2010. Copper in diseases and treatments, and copper-based anticancer strategies. Med. Res. Rev. 30 (4), 708–749.

Wadt, W.R., Hay, P.J., 1985. Ab initio effective core potentials for molecular calculations. Potentials for main group elements Na to Bi. J. Chemical Phys. 82 (1), 284–298.

Wang, H., Joseph, J.A., 1999. Quantifying cellular oxidative stress by dichlorofluorescein assay using microplate reader. Free Radical Biol. Med. 27 (5–6), 612–616. https://doi.org/10.1016/s0891-5849(99)00107-0.

Xie, H., Kang, Y.J., 2009. Role of copper in angiogenesis and its medicinal implications. Curr. Med. Chem. 16 (10), 1304–1314.

Xu, S., Yao, H., Luo, S., Zhang, Y.K., Yang, D.H., Li, D., Wang, G., Hu, M., Qiu, Y., Wu, X., Yao, H., 2017. A novel potent anticancer compound optimized from a natural oridonin scaffold induces apoptosis and cell cycle arrest through the mitochondrial pathway. J. Med. Chem. 60 (4), 1449–1468. https://doi.org/10.1021/acs.jmedchem.6b01652.

Yousuf, I., Arjmand, F., Tabassum, S., Toupet, L., Khan, R.A., Siddiqui, M.A., 2015. Mechanistic insights into a novel chromone-appended Cu (II) anticancer drug entity: in vitro binding profile with DNA/RNA substrates and cytotoxic activity against MCF-7 and HepG2 cancer cells. Dalton Trans. 44 (22), 10330–10342. https://doi.org/10.1039/C5DT00770D.

Yu, H., Yang, Y., Li, Q., Ma, T., Xu, J., Zhu, T., Xie, J., Zhu, W., Cao, Z., Dong, K., Huang, J., 2016. Ternary dinuclear copper (II) complexes of a reduced schiff base ligand with diimine coligands: DNA binding, cytotoxic cell apoptosis, and apoptotic mechanism. Chem. Biol. Drug Des. 87 (3), 398–408. https://doi.org/10.1111/cbdd.12669.

Zimmermann, T., Burda, J.V., 2010. Cisplatin interaction with amino acids cysteine and methionine from gas phase to solutions with constant pH. Interdisciplinary Sciences: Computational Life Sciences 2 (1), 98–114. https://doi.org/10.1007/s12539-010-0094-x.